AGU PUBLICATIONS

Radio Science

RESEARCH ARTICLE
10.1002/2014RS005503

Special Section:
URSI Symposium on Radiowave Propagation and Remote Sensing, 2013

Investigating raindrop shapes, oscillation modes, and implications for radio wave propagation

M. Thurai[1], V. N. Bringi[1], A. B. Manić[1], N. J. Šekeljić[1], and B. M. Notaroš[1]

[1]Department of Electrical and Computer Engineering, Colorado State University, Fort Collins, Colorado, USA

Abstract Studies of raindrop shapes, oscillation modes, and implications for radio wave propagation are presented. Drop shape measurements in natural rain using 2-D video disdrometers (2DVDs) are discussed. As a representative exception to vast majority of the cases where the "most probable" shapes conform to the axisymmetric (2,0) oscillation mode, an event with a highly organized line convection embedded within a larger rain system is studied. Measurements using two collocated 2DVD instruments and a C-band polarimetric radar clearly show the occurrence of mixed-mode drop oscillations within the line, which in turn is attributed to sustained drop collisions. Moreover, the fraction of asymmetric drops determined from the 2DVD camera data increases with the calculated collision probability when examined as time series. Recent wind-tunnel experiments of drop collisions are also discussed. They show mixed-mode oscillations, with (2,1) and (2,2) modes dramatically increasing in oscillation amplitudes, in addition to the (2,0) mode, immediately upon collision. The damping time constant of the perturbation caused by the collision is comparable to the inverse of the collision frequency within the line convection. Scattering calculations using an advanced method of moments numerical technique are performed to accurately and efficiently determine the pertinent parameters of electrically large oscillating raindrops with asymmetric shapes needed for radio wave propagation. The simulations show that the scattering matrix and differential reflectivity of drops are dependent on the particular oscillation modes and different time instants within the oscillation cycle. The technique can be utilized in conjunction with 3-D reconstruction of drop shapes from 2DVD data.

Key Points:
- Collision induced mixed-mode drop oscillations
- 2DVD and polarimetric-radar measurements and wind-tunnel experiments
- Method-of-moments scattering calculations of asymmetric drops

Correspondence to:
M. Thurai,
merhala@engr.colostate.edu

Citation:
Thurai, M., V. N. Bringi, A. B. Manić, N. J. Šekeljić, and B. M. Notaroš (2014), Investigating raindrop shapes, oscillation modes, and implications for radio wave propagation, *Radio Sci.*, *49*, 921–932, doi:10.1002/2014RS005503.

Received 30 APR 2014
Accepted 16 SEP 2014
Accepted article online 19 SEP 2014
Published online 20 OCT 2014

1. Introduction

Drop shapes in rain and their oscillation modes are important parameters needed for evaluating radio wave propagation effects in rain and the polarization dependence, for terrestrial and satellite systems operating in the microwave and millimeter wave frequencies [*Oguchi*, 1983; *Allnutt*, 1989; *Okamura and Oguchi*, 2010]. In the case of linear polarization, for example, the specific attenuation for horizontal and vertical polarizations will differ because of the nonspherical shapes of raindrops, the former being higher than the latter because the "most probable" shapes have the horizontal dimension larger than the vertical and the drops tend to fall with their symmetry axes almost aligned with the local vertical. Drop shapes and oscillation modes are even more important for satellite systems, which utilize orthogonal polarizations within a given bandwidth in order to increase the efficiency of the radio spectrum and hence require information on depolarization effects along their atmospheric propagation paths [*Brussaard*, 1976; *Martellucci and Paraboni*, 1998; *Aresu et al.*, 1994; *Amaya-Byrne*, 1995; *COST Action 255*, 2002; *Van de Kamp*, 2004].

Drop shapes and their oscillation modes also play a central role in rainfall remote sensing using polarimetric radar [*Bringi and Chandrasekar*, 2001; *Doviak and Zrnić*, 1993]. The retrieval of raindrop size distributions (DSDs) and the subsequent development of algorithms for estimating rainfall rates from polarimetric radar observations need—as input—the most probable shapes and their variations due to oscillations. For C- and X-band radars, an additional consideration relates to attenuation correction schemes, which again requires shape information [*Gourley et al.*, 2009].

Previous work on drop shapes has ranged from laboratory and wind tunnel measurements (see *Beard et al.* [2010] for a recent review) to inferences from polarimetric data [*Goddard et al.*, 1982], as well as theoretical modeling studies [for example, *Beard and Chuang*, 1987]. Additionally, the 2-D video disdrometer (2DVD) [*Schönhuber et al.*, 2000, 2008] has been utilized to determine drop shapes from an artificial rain experiment [*Thurai and Bringi*, 2005; *Thurai et al.*, 2007], as well as in natural rain (as reported by *Beard et al.* [2010], for example).

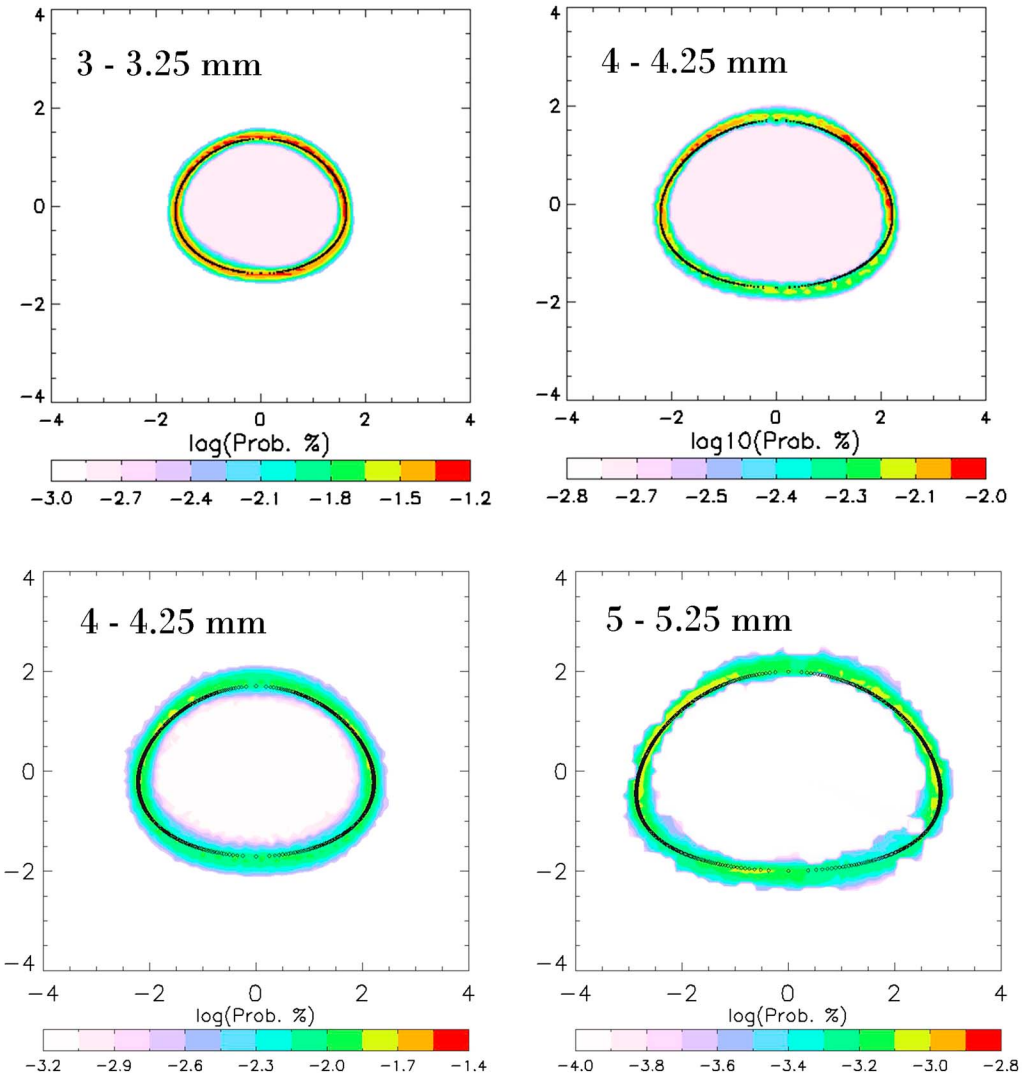

Figure 1. Drop shape measurements in natural rain from 2DVD for drop equivolume diameters of (top left) 3–3.25 mm and (top right) 4–4.25 mm from SE Queensland, Australia, and for (bottom left) 4–4.25 mm and (bottom right) 5–5.25 mm from Huntsville, Alabama. All dimensions (in *x* and *y*) are in mm, and the black line represents the most probable shapes given in equation (1) of *Thurai et al.* [2007].

In terms of scattering models and techniques, the T-matrix method [*Mishchenko et al.*, 2002] and the discrete dipole approximation (DDA) method [*Draine and Flatau*, 1994] are the two conventionally and almost exclusively used tools in hydrometeor scattering analysis. However, drops undergoing mixed-mode oscillations, in general, are not rotationally symmetric (axisymmetric), and practically all working T-matrix tools are able to calculate the scattering properties of rotationally symmetric particles only. The major advantage of the DDA method is that it can be applied to arbitrarily shaped (asymmetric) drops, but its numerical accuracy is relatively low, and computational costs are extremely high.

Our current investigations on drop shapes mostly involve field campaigns with 2DVDs and polarimetric radars [*Thurai et al.*, 2013c]. Furthermore, results from experiments conducted using an advanced wind tunnel facility [*Pruppacher*, 1988; *Szakáll et al.*, 2009] are also being utilized [*Thurai et al.*, 2013a]. In this paper, we present our continued studies of raindrop shapes, oscillation modes, and implications for radio wave propagation and discuss the occurrence of mixed-mode oscillations under some special circumstances. We also show and discuss how (a) shape information, including asymmetric shapes of drops due to collision-induced drop oscillations, can be inferred from activities encompassing 2DVD and polarimetric radar natural rain field measurements and wind tunnel artificial rain experiments in a synergistic manner and (b) scattering

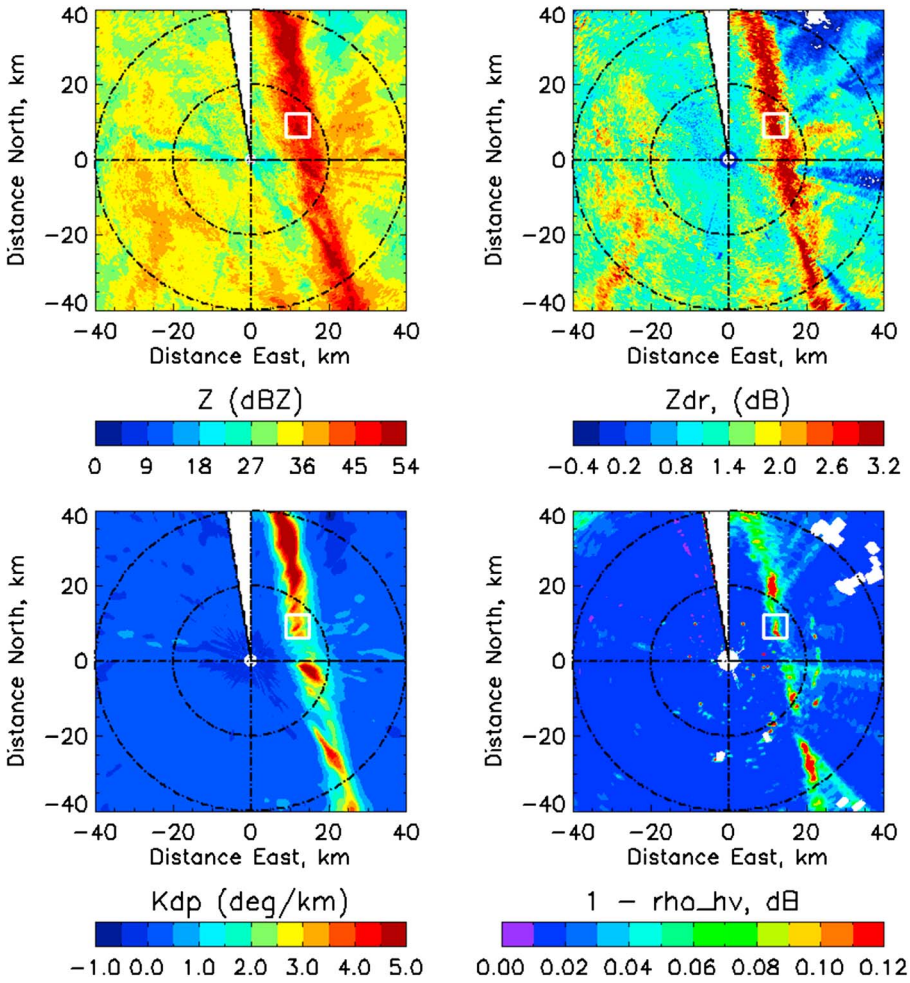

Figure 2. PPI scan from ARMOR radar at 03:40 UTC during the 25 December 2009 event. The 2DVD location is indicated with a white square. The line convection can be seen to have (top left) high reflectivities (>50 dBZ), (top right) high Z_{dr} (>3.2 dB), (bottom left) high K_{dp} (>5°/km), and (bottom right) regions with lower than expected ρ_{hv} (<0.88). Note that the last panel is given in terms of $1 - \rho_{hv}$ for more clarity.

calculations using an advanced numerical technique based on the method of moments [*Djordjević and Notaroš*, 2004] can be used to accurately and efficiently determine the pertinent parameters of asymmetric electrically large hydrometeors needed for rainfall remote sensing, as well as radio wave propagation.

2. Raindrop Shape Measurements and Polarimetric Radar Observations

Drop shapes from 2DVD measurements in natural rain have been determined at numerous locations including Huntsville (Alabama, USA), Brisbane (Australia), and Okinawa (Japan). A thorough examination of the 2DVD camera data has indicated that in the vast majority of cases, the most probable shapes conform to those arising from the axisymmetric (2,0) mode [*Beard et al.*, 2010]. In all cases, drop images of over 90% of the moderate-to-large-sized drops could be successfully deskewed. Two-dimensional views of such rotationally symmetric drops measured in natural rain are shown in Figure 1.

However, there have been a few important exceptions. A recent study (details given by *Thurai et al.* [2013b] and *Thurai and Bringi* [2013]) using two collocated 2DVD instruments and the C-band polarimetric radar, Advanced Radar for Meteorological and Operational Research (ARMOR) (University of Alabama in Huntsville (UAH) Advanced Radar for Meteorological and Operational Research) [*Petersen et al.*, 2007; *Crowe et al.*, 2012], in Huntsville, Alabama, USA, has clearly shown that in an event (which occurred on 25 December 2009) that had a highly organized line convection embedded within a larger rain system, mixed-mode oscillations were

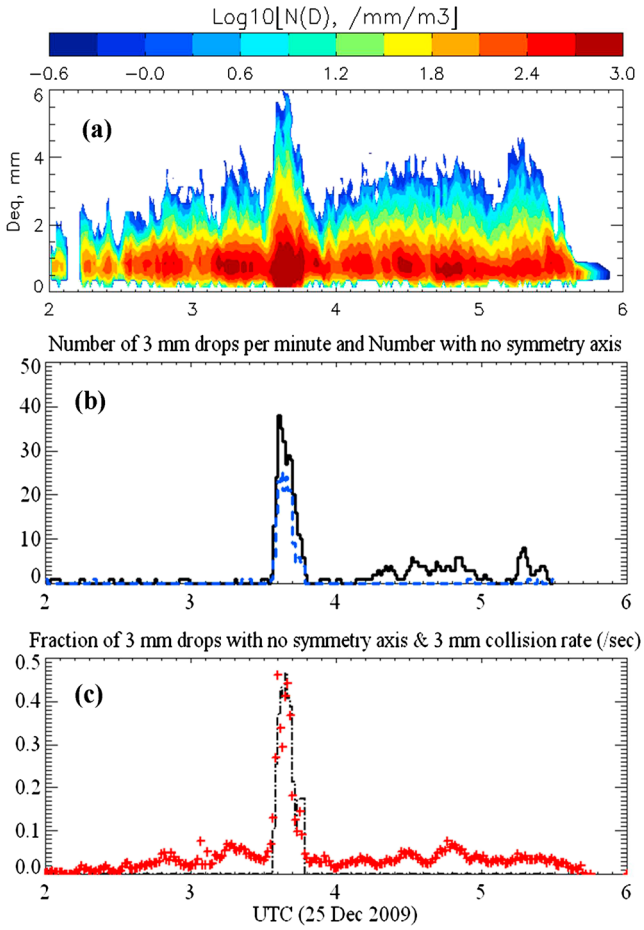

Figure 3. (a) One minute DSD for the 25 December 2009 event. (b) Number of 3 mm drops measured per minute in black and the number with no symmetry axis in blue. (c) Fraction of 3 mm drops with no symmetry axis in black and calculated collision rate for a single 3 mm drop with all smaller drops. Note that the small drop adjustments using the single-camera data have been made for $D < 0.5$ mm for the collision rate calculations.

occurring within the intense rain shafts, which in turn were attributed to frequent, and sustained, drop collisions. Inferences were made from the 2DVD camera data, which showed that over 30% of the larger-sized drops (3 mm drop diameter and higher) were undergoing asymmetric mode oscillations when the line passed over the 2DVD site; i.e., their image projections were nondeskewable. Additionally, the C-band radar data showed much higher than expected differential attenuation within the line, as well as reduced copolar correlation coefficient values (ρ_{hv}), which were significantly lower than those expected due to the wide spectral width of the measured DSDs alone. Figure 2 shows the PPI scan from ARMOR at 03:40 UTC. Copolar attenuation (CPA) and differential attenuation correction procedures have been applied to both reflectivity (Z_h) and differential reflectivity (Z_{dr}), but even so, beyond the line to the east, negative Z_{dr} can be seen despite the attenuation correction procedure (assuming our "reference" drop shapes, as given in equations (1) and (2) of *Thurai et al.* [2007], and assuming rotational symmetry, with the axis of symmetry along the local zenith). High specific differential phase (K_{dp}) values are seen indicating high rain intensities within the line, and the ρ_{hv} shows a "dip" which is lower than the expected values arising from the wide DSDs alone (again assuming our reference drop shapes). The white "square" denotes the 2DVD location, and as can be seen, the convection line lies directly above it at 03:40 UTC.

It is at this time that the 2DVD data showed the presence of large drops and high concentration of small drops. This can be seen from Figure 3a, which shows the measured 1 min DSDs as time series. Note that some adjustments of drop concentration have been made for the small and tiny drops (for drop diameters < 0.4 mm) because there are mismatching problems between the two 2DVD camera images for such small drops. However, recently, it has become possible to adjust these concentrations using single-camera data. The drop size for these small drops is determined from the maximum scan length (number of pixels shadowed in the horizontal) from one of the camera images, and the vertical dimension is determined assuming that their shapes are essentially spherical, which is a good approximation for drop diameters less than 0.4 mm. The fall speed is estimated by knowing the vertical dimension, the number of scan lines, and the line scan frequency. Previous comparisons of such adjustments with those derived from the Precipitation Occurrence Sensor System [*Sheppard*, 1990] have shown very good agreement for 0.1 to 0.4 mm range.

Figure 3b shows the number of 3 mm drops (as an example, $D = 3$ mm) measured per minute and the number with no symmetry axis in blue, and Figure 3c shows the fraction of 3 mm drops with no symmetry axis—again for the 3 mm drops—as well as the corresponding collision rate for a single 3 mm drop with all smaller drops (of diameter d), calculated using a relatively simple collision model based on equation (1) of

Johnson and Beard [1984], which in essence is based on the product of the sweep out area proportional to $(D+d)^2$ and the fall speed difference $v(D)-v(d)$ weighted by the concentration of the small drops. The aforementioned adjustment of the concentration of small drops has been used in these calculations.

From Figures 3b and 3c, we can see that as the collision rate increases, the fraction of asymmetric drops also increases, strongly implying that the collision-induced drop oscillations are taking place within the narrow line convection and that such oscillations are giving rise to a significant fraction of asymmetrically shaped drops at a given instant in time. In the next two sections, we discuss the various oscillation modes and wind tunnel experiments conducted to examine the collision-induced drop oscillations.

3. Raindrop Oscillations

The wind tunnel measurements of *Szakáll et al.* [2009] allow for calculating the apparent axis ratio of an oscillating drop as it goes through many cycles of oscillation. According to *Beard and Kubesh* [1991], the oscillation of raindrops can be characterized via different (*n*,*m*) modes and described in a spherical coordinate system (defined in Figure 6 given later in section 5) as

$$r_{n,m}(t,\theta,\phi) = r_0 + A\sin(\omega t)P_{n,m}(\theta)\cos(m\phi) \tag{1}$$

where $r_0 = D/2$ is the "mean" radius of the drop, D is the equivolume drop diameter, A is the oscillation amplitude, and $P_{n,m}(\theta)$ are the Legendre polynomials. Recently, techniques based on the time variation of the apparent axis ratio and other image characteristics—such as circumscribed box and projected area—have been developed for the wind-tunnel measurements [*Szakáll et al.*, 2014] to identify the three distinct fundamental modes: (i) the axisymmetric (spherical harmonic $n=2$, $m=0$) mode, (ii) the transverse (2,1) mode, and (iii) the horizontal (2,2) mode. For these modes, Legendre polynomial functions are

$$P_{n,m}(\theta) = \begin{cases} 0.5\,(3\cos^2\theta - 1) & (n,m) = (2,0) \\ 3\cos\theta\sin\theta & (n,m) = (2,1) \\ 3\sin^2\theta & (n,m) = (2,2) \end{cases} \tag{2}$$

Figure 4 depicts the three fundamental modes at two different times within the oscillation cycle. From a frequency analysis of the time series of these image characteristics [*Szakáll et al.*, 2014], it was found that the dominant mode of oscillation for $D > 2.5$ mm was the axisymmetric, "oblate-prolate" mode, with the small-amplitude transverse modes also being mixed in [e.g., *Foote*, 1973; *Beard*, 1984; *Feng and Beard*, 1991]. The highly symmetric axis ratio distributions (about the equilibrium value) from the 80 m fall experiment [*Thurai and Bringi*, 2005] also support, indirectly, the dominance of the axisymmetric mode for $D > 2$ mm [see also *Kubesh and Beard*, 1993]. Review articles by *Beard et al.* [2010] and *Szakáll et al.* [2010], and the references contained therein give a fuller description of drop shapes and oscillation modes. Thus, the background oscillation state of drops with $D > 2$ mm (in the absence of collisions) is the (2,0) mode.

4. Raindrop Collisions

To investigate the collision-induced drop oscillations further, the vertical wind tunnel facility, based in Mainz, Germany, has been utilized. Details can be seen in *Szakáll et al.* [2014] and *Thurai et al.* [2013a]. More than 130 cases were recorded with a high-speed digital video camera. Many of the recorded collision events had to be abandoned because the drops were not in the focal plane of the camera; however, it was possible to analyze around 40 collision events. Among these, there were 27 events resulting in drop coalescence, while the remaining ones resulted in noncoalescence collision.

The sizes of the colliding drop pairs were chosen to be typical for real atmospheric conditions; i.e., for the collector drops, they were in the 2.4–3 mm drop diameter range, while the small droplets had sizes of around 0.5 mm. Such combination was approximately based on Figure 9 of *Johnson and Beard* [1984], which shows the maximum rate of collisional energy input for collisions between a 4 mm drop and 0.6 mm drop. In each case, the collector drop was freely floated inside the wind tunnel until a small droplet (injected from below) coming from the upstream side of the larger drop collided with it. Data analysis clearly showed that the larger drop—upon collision—undergoes mixed-mode oscillations, with (2,1) and (2,2) modes dramatically increasing in oscillation amplitudes, in addition to the (2,0) mode. The perturbation caused by the collision lasts for over several hundred milliseconds before effectively getting damped out and reverting

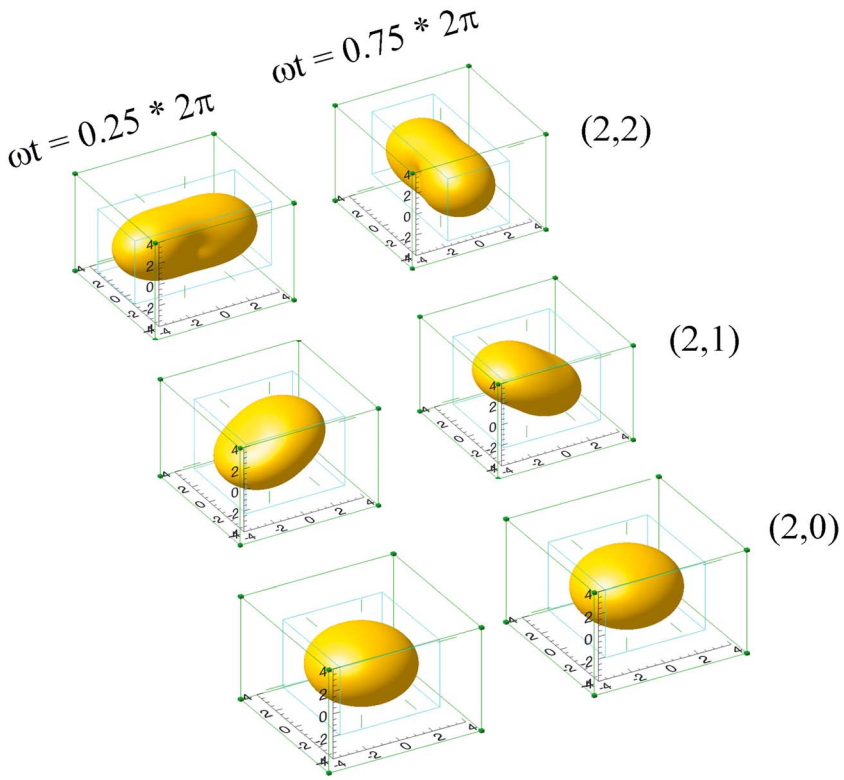

Figure 4. Three-dimensional views of the three fundamental oscillation modes (all units are in millimeter), for two phases of the oscillation cycle given by (i) $\omega t = 0.25 \times 2\pi$ and (ii) $\omega t = 0.75 \times 2\pi$. Equations (1) and (2) have been used to generate these figures. Note that $D = 2r_0 = 6$ mm, where D is the equivolume drop diameter, and $A = 0.1r_0$ (10% relative amplitude of oscillation).

to its usual (2,0) oscillation mode as the dominant mode. A typical example of the "apparent" axis ratio variation of a drop during a collision-coalescence process is presented in Figure 5. The collision occurs at ~250 ms. The time moment of the collision is coupled with a large-axis ratio variation. The multimode oscillation of the drops is obvious from the beating in the time series. Around 450 ms after collision, the perturbation caused by the collision is effectively damped out by viscous decay, and the drop is oscillating with the same amplitude as before collision. Note that the time constant for viscous decay of a spherical drop oscillating in its fundamental mode is also 0.4 s for $D = 3$ mm using, for example, equation (4) of *Johnson and Beard* [1984]. Since the collision rates in moderate-to-intense rain rates can be on the order of 0.3 s^{-1} [*Rogers*, 1989], or even higher by a factor of 2.5 for "clustered rain" [*McFarquhar*, 2004], it is possible, in principle, to sustain multimode oscillations against viscous dissipation.

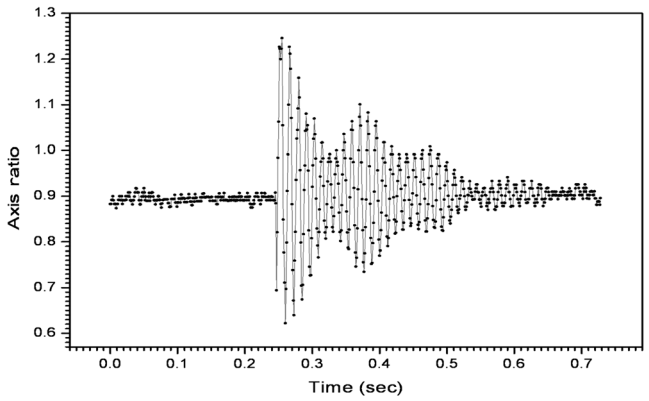

Figure 5. A typical example of the axis ratio variation of a drop during a collision-coalescence process. The collector drop (~2.5 mm) was freely floating in the wind tunnel until a small droplet (around 0.5 mm) from the upstream side of the drop collided with it at 250 ms. The time moment of the collision is coupled with a large-axis ratio variation. The multimode oscillation of the drops is obvious from the "beating" in the time series. Around 450 ms after collision, the perturbation caused by the collision is effectively damped out, and the drop is oscillating with the same amplitude as before the collision.

By performing a time series analysis of the apparent image characteristics, the frequency spectra of the oscillations of drops before, during,

and after the collision processes were determined (again details are given by *Szakáll et al.* [2014] and *Thurai et al.* [2013a]). In both the coalescing and noncoalescing cases, the (2,0) mode was found to be the most pronounced oscillation mode before collision. After collision, the (2,1) mode was found to become much more active, and in fact, it becomes the dominating oscillation mode, i.e., the mode which determines the apparent axis ratio variation. Furthermore, in the coalescing case, the amplitude of the (2,2) mode was found to be significantly larger.

The fact that the damping time constant of the decay of the mixed-mode oscillations is of the order of several hundred milliseconds must mean that if in real atmospheric conditions the collision frequency has similar "time constant," then sustained drop collisions can cause significant fraction of the drops at any instant in time to be in mixed-mode oscillation state (and not have rotational axis of symmetry). Referring back to the aforementioned event (Figures 2 and 3), the most probable explanation is that drops are undergoing mixed-mode oscillations within the line convection region and that these are probably due to drop collisions, e.g., 3 mm drops with tiny drops (probable scenario according to literature). If such collisions occur typically at a rate of 0.2 s^{-1} (for 3 mm drops in a 55 dBZ reflectivity rain column) [from *Rogers*, 1989], then it is conceivable that collisions can sustain drop oscillations (against viscous dissipation) for a significant fraction of the 3 mm drops. This has also been hypothesized by *Jameson and Durden* [1996] from airborne measurements of copolar and cross-polar backscatter from tropical storms. For the event given in Figures 2 and 3, high rain intensity confined within the narrow line convection would significantly increase the likelihood of drop collisions. Moreover, in the case of rain clustering [see, for example, *Jameson and Kostinski*, 1999], which may well be the case within the embedded line convection in this event, drop collision rates can increase by a significant factor [*McFarquhar*, 2004]. *Johnson and Beard* [1984] have calculated the fraction of drops having significant oscillation amplitudes (collision-induced) for various large drop diameters and rain rates. For example, in their Table 2, this fraction is 44% for 3 mm sized drops for a rain rate of 100 mm/h. In our example event, the maximum rain rates measured by the 2DVDs were around 75 mm/h.

5. Scattering Calculations for Asymmetric Raindrops

Drops undergoing mixed-mode oscillations are likely to not have rotational symmetry at any given instant in time, and for such cases, traditional scattering analysis techniques such as the well-established version of the T-matrix method [*Mishchenko et al.*, 2002] cannot be readily utilized. Techniques such as discrete dipole approximation (DDA) [see, for example, *Draine and Flatau*, 1994; *Teschl et al.*, 2013] are more suitable, but the numerical accuracy of the DDA method is relatively low, and improves slowly with increasing the number of dipoles, which makes the DDA computation very time consuming. In addition, the DDA code may not converge for any reasonable predefined accuracy and number of iteration steps in some cases with high-contrast dielectric materials and large electrical sizes of particles [*Chobanyan et al.*, 2013a]. Finally, the DDA needs to repeat the entire calculation for each new excitation, since it uses an iterative solution and the system of equations has to be solved for each excitation vector separately. Instead, we consider here a more accurate, efficient, and versatile numerical technique based on the method of moments (MOM) in the surface integral equation (SIE) formulation, implemented as a higher-order technique [*Notaroš*, 2008]. This technique enables efficient scattering matrix calculations of asymmetric hydrometeors of electrically large (compared to wavelength) sizes.

According to the MOM-SIE approach, the surface of a hydrometeor is modeled using generalized curved Lagrange interpolation polynomial (L) quadrilateral patches of arbitrary geometrical orders K_u and K_v, shown in Figure 6, and electric and magnetic equivalent surface currents of densities $\mathbf{J}_s$ and $\mathbf{M}_s$ over quadrilaterals are approximated by hierarchical vector basis functions $\mathbf{f}$ of arbitrary expansion orders N_u and N_v [*Djordjević and Notaroš*, 2004],

$$\mathbf{r}(u,v)=\sum_{k=0}^{K_u}\sum_{l=0}^{K_v}\mathbf{r}_{kl}L_k^{K_u}(u)L_l^{K_v}(v),\quad \mathbf{J}_s=\sum_{i=0}^{N_u}\sum_{j=0}^{N_v}\alpha_{ij}\mathbf{f}_{ij}(u,v),\quad \mathbf{M}_s=\sum_{i=0}^{N_u}\sum_{j=0}^{N_v}\beta_{ij}\mathbf{f}_{ij}(u,v),\ -1\le u,v\le 1 \tag{3}$$

where α and β are unknown current distribution coefficients (unknowns), determined by the MOM solution of surface integral equations (SIEs) based on boundary conditions for electric and magnetic fields on the hydrometeor surface using a fast direct solver.

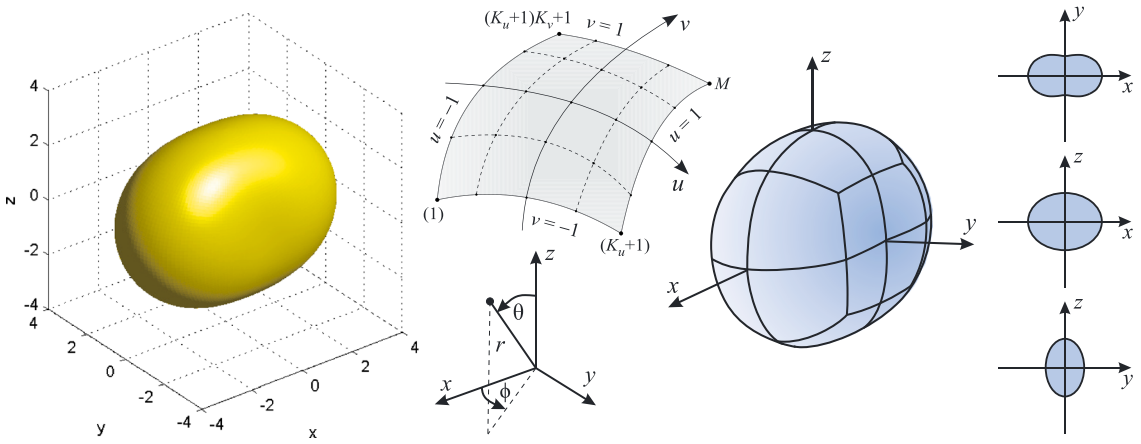

Figure 6. (left) Raindrop shape (all units are mm) corresponding to oscillation mode (2,2) at $\omega t = \pi/2$ in equation (1) ($D = 2r_0 = 6$ mm, $A = 0.1r_0$). (middle) Generalized curved parametric quadrilateral patch, defined in equation (3), for higher-order MOM-SIE modeling, with surface currents approximated by polynomial basis functions given in equation (3) and spherical coordinate system for defining oscillating raindrop modes. (right) MOM-SIE model of the oscillating raindrop in the left using 24 large patches with $K_u = K_v = 4$ and $N_u = N_v = 3$ (864 unknowns).

Figure 6 describes the higher-order MOM-SIE modeling of a 6 mm oscillating raindrop, with $r_0 = 3$ mm and $A = 0.1r_0$ in equation (1), in the horizontal fundamental oscillation mode (2,2) at a time instant defined by $\omega t = \pi/2$ within the oscillation cycle (Figure 4). Note the geometrical deviation of the drop when compared to the spherical shape. MOM-SIE model using 24 large curved quadrilateral patches with $K_u = K_v = 4$ and $N_u = N_v = 3$ in equation (3) is depicted in Figure 6, which results in a total of 864 unknowns for the simulation. Figure 7 shows the MOM results for the monostatic (back) differential reflectivity (Z_{dr}) of the drop at the frequency $f = 3$ GHz, at which the complex dielectric constant of rainwater is $\varepsilon_r = 80 - j20$. The results are obtained for different incidence/scattering angles $\phi_{inc} = \phi_{scat}$ in the plane $\theta_{inc} = \theta_{scat} = 90°$ (0° radar elevation angle—see the spherical coordinate system in Figure 6). To cross validate the results, computations on three MOM models are carried out: (1) MOM-SIE model with 24 large patches (Figure 6), (2) MOM-SIE model using 2400 small quadrilateral patches with $K_u = K_v = 1$ and $N_u = N_v = 1$ (9600 unknowns), and (3) MOM-VIE (volume integral equation) model using 27 large curved hexahedral volume elements with volume polarization current [*Chobanyan et al.*, 2013b] (6400 unknowns). Note that the MOM-VIE technique is very suitable for the simulations of inhomogeneous (e.g., melting ice) scatterers. We also compare the MOM solutions to the results obtained by the DDA method using discrete dipole scattering 7.2 code by *Draine and Flatau* [2012].

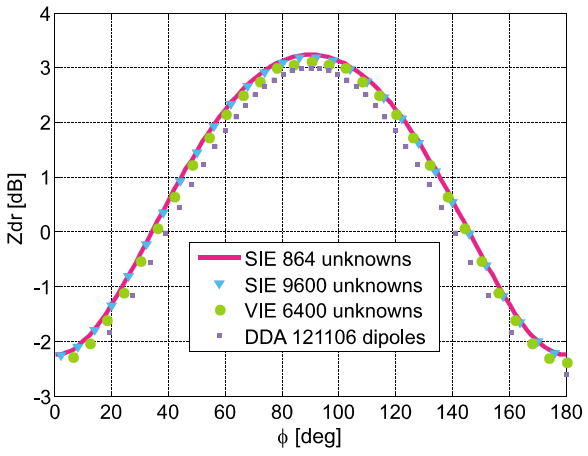

Figure 7. Monostatic (back) differential reflectivity (Z_{dr}) in the *x-y* plane for the oscillating raindrop in Figure 6 (frequency $f = 3$ GHz, complex dielectric constant $\varepsilon_r = 80 - j20$) computed by the MOM-SIE on two models, MOM-VIE, and DDA code, with the first MOM-SIE solution (model shown in Figure 6) being more than 1000 times faster than the DDA solution [*Sekeljic et al.*, 2014].

We observe from Figure 7 an excellent agreement of the three sets of MOM results and their good agreement with the DDA results. For this specific case, as expected, the maximum Z_{dr} occurs at $\phi = 90°$. Note that Z_{dr} of the drop is rather different from that of an equivolume sphere, for which $Z_{dr} = 0$ dB for all incidence angles. Note also that, generally, the dependence of Z_{dr} on incidence angles θ_{inc} and ϕ_{inc} is quite different for different oscillation modes and different time instants within the oscillation cycle, in Figure 4. The total computation times for all 91 directions

Table 1. MOM-SIE Simulation Results for Complex Forward Scattering Amplitudes of an Oscillating Raindrop in Mode (2,2) at $f = 20$ GHz[a]

θ_{inc} (°)	ϕ_{inc} (°)	θ_{scat} (°)	ϕ_{scat} (°)	Re{S_{hh}} (10^{-3})	Im{S_{hh}} (10^{-3})	Re{S_{hv}} (10^{-3})	Im{S_{hv}} (10^{-3})	Re{S_{vv}} (10^{-3})	Im{S_{vv}} (10^{-3})	Re{S_{vh}} (10^{-3})	Im{S_{vh}} (10^{-3})
110	0	70	180	0.8566	−1.8068	0.0000	0.0000	0.6373	−2.5554	0.0000	0.0000
110	9	70	189	0.8478	−1.8555	0.0377	0.0801	0.6452	−2.5650	0.0377	0.0801
110	18	70	198	0.8200	−1.9991	0.0743	0.1531	0.6676	−2.5926	0.0743	0.1531
110	27	70	207	0.7692	−2.2278	0.1078	0.2126	0.7026	−2.6376	0.1078	0.2126
110	36	70	216	0.6909	−2.5239	0.1351	0.2525	0.7469	−2.6980	0.1351	0.2525
110	45	70	225	0.5852	−2.8624	0.1522	0.2684	0.7960	−2.7695	0.1521	0.2685
110	54	70	234	0.4596	−3.2136	0.1546	0.2579	0.8454	−2.8474	0.1545	0.2580
110	63	70	243	0.3276	−3.5396	0.1391	0.2214	0.8907	−2.9239	0.1391	0.2214
110	72	70	252	0.2098	−3.8044	0.1057	0.1619	0.9259	−2.9870	0.1057	0.1620
110	81	70	261	0.1282	−3.9779	0.0571	0.0855	0.9494	−3.0307	0.0571	0.0855
110	90	70	270	0.0983	−4.0381	0.0000	0.0000	0.9570	−3.0453	0.0000	0.0000

[a]The results are given for the FSA convention, $\omega t = \pi/2$, $D = 6$ mm, $A = 0.1r_0$, $\varepsilon_r = 36 - j36$, and all four combinations of the horizontal (*h*) and vertical (*v*) polarizations of the incident and scattered waves (for example, S_{hv} corresponds to the *v* incident and *h* scattered polarizations). Angles θ and ϕ are defined as in Figure 6. Note that $\theta_{inc} = 110°$ and $\theta_{scat} = 70°$ correspond to an earth station elevation of 20°.

of incidence are 2 min 23 s, 5 min 26 s, 5 min 10 s, and as large as 40 h 2 min 3 s for the MOM-SIE model (1), MOM-SIE model (2), MOM-VIE, and DDA analyses, respectively, on a very modest computer (PC Intel® Core™2 Quad Q9550 2.83 GHz 4 GB random access memory). This demonstrates that the higher-order MOM techniques are dramatically more efficient than the DDA technique [see also *Chobanyan et al.*, 2013a], while the T-matrix method cannot be used at all in this example if the asymmetric shape of the drop is to be taken accurately into account.

Next, we perform the higher-order MOM-SIE analysis of the same 6 mm oscillating raindrop but at the frequency $f = 20$ GHz (typical earth-space communication band), where the complex dielectric constant of the drop is $\varepsilon_r = 36 - j36$ for 20°C [*Ray*, 1972], and in the forward scattering configuration. The simulated MOM-SIE model uses 864 curved quadrilateral patches with $K_u = K_v = 2$ and $N_u = N_v = 2$ (13,824 unknowns). The results for complex forward scattering amplitudes of the drop with $r_0 = 3$ mm and $A = 0.1r_0$ in the horizontal oscillation mode (2,2) at $\omega t = \pi/2$ computed for the horizontal and vertical polarizations of the incident wave are given in Table 1, respectively. The scattering amplitudes are computed in accordance to the notation constituting the FSA (forward scattering amplitude) convention [*Bringi and Chandrasekar*, 2001]. We keep the elevation angle for both the incident and the forward scattering directions fixed, specifying $\theta_{inc} = 110°$ and $\theta_{scat} = 70°$ (both of which correspond to an earth station elevation angle of 20°), vary the incident azimuthal angle with uniform steps of 9° in the range $0° \le \phi_{inc} \le 90°$ (we consider only one quarter of the full azimuthal range because the results in the other quarters are the same), for which the corresponding forward scattering range is $180° \le \phi_{scat} \le 270°$, and compute the 2×2 scattering matrix for each azimuthal angle.

Then, for comparison, we redo the simulations for the rotationally symmetric (2,0) mode, where, of course, there is no azimuthal dependence and show the forward scattering results in Table 2. We observe from Tables 1 and 2 the considerable differences in the complex scattering amplitudes between the (2,2) and (2,0) modes, particularly when ϕ_{inc} approaches 90°. Additionally, the MOM-SIE results for the (2,0) mode are validated against those obtained using the T-matrix method, which is possible in this case of a rotationally symmetric drop shape, and an excellent agreement of the two sets of numerical results is observed in Table 2.

To generate MOM-SIE models for the computation of scattering from raindrops in natural rain, it is possible to reconstruct the 3-D shape of the asymmetric and symmetric drops using a spline interpolation procedure

Table 2. Forward Scattering Results for the (2,0) Mode of the Oscillating Raindrop[a]

Analysis Done by	θ_{inc} (°)	ϕ_{inc} (°)	θ_{scat} (°)	ϕ_{scat} (°)	Re{S_{hh}} (10^{-3})	Im{S_{hh}} (10^{-3})	Re{S_{hv}}, Im{S_{hv}}	Re{S_{vv}} (10^{-3})	Im{S_{vv}} (10^{-3})	Re{S_{vh}}, Im{S_{vh}}
MOM-SIE method	110	0	70	180	0.7796	−2.5603	0.0000	0.5597	−2.9789	0.0000
T-matrix method	110	0	70	180	0.7805	−2.5660	0.0000	0.5587	−2.9883	0.0000

[a]The results are given for the same raindrop and frequency as in Table 1 but in the rotationally symmetric mode. Validation of MOM-SIE results against the T-matrix method is also shown.

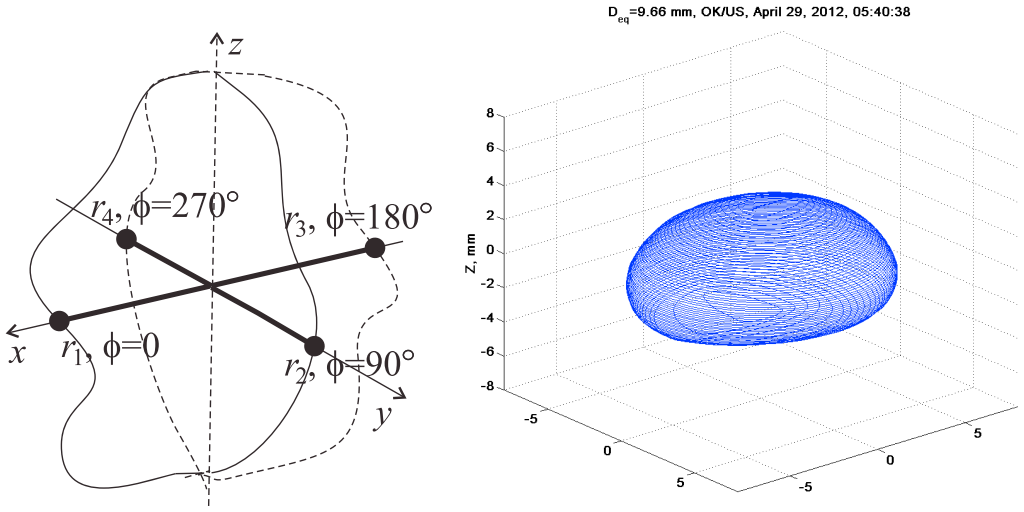

Figure 8. (left) Geometrical reconstruction of 3-D raindrop shapes from 2DVD contours—determination of four bound points of 2-D orthogonal contours that are used to create a four-point-based curvilinear spline in each z = constant plane as an approximation of the drop contour for that coordinate z (this is repeated with increments Δz). (right) An example plot of a preliminary 3-D reconstruction of a very large drop (D = 9.7 mm) constructed from the two projected contours recorded by the 2DVD's two orthogonal camera data. The x, y, and z axes all have units of millimeter.

applied to 2-D contours of a raindrop in two mutually orthogonal cross sections obtained by the two cameras of the 2DVD. Appropriate corrections can be applied for the effect of the horizontal component of the drop velocity on the two orthogonal contours. We start with four points obtained from the two 2-D contours, with the determination of these points being illustrated in Figure 8 (left), where the intersections of planes xz and yz with the object in the plane $z = 0$ give four points (these four points determine the bound points of the two cross sections of the object along the x and y axes), and this is repeated for every coordinate z with certain increments Δz. Using these four points, it is possible to create a four-point-based curvilinear spline in each z = const plane in order to generate the contour of the 3-D object for that coordinate z and then connect these contours into a 3-D surface.

A 3-D reconstruction of a very large drop is shown in Figure 8 (right). It represents one of the largest drop recorded by the 2DVD, with a drop equivolume diameter of 9.7 mm. The drop has a symmetry axis, and the flattening of its base is clearly visible. The event was captured also by an operational S-band weather radar as well as an X-band radar, both with polarimetric capability, and has been undergoing further analysis [*Thurai et al.*, 2014]. Note that for drops with asymmetric shapes, the drop horizontal velocity is not computable from the 2DVD measurements, and for such cases, the horizontal velocity determined from a drop of similar size closest in time can be used for the correction (deskewing) procedure.

The reconstructed shapes—after a suitable generation of the surface mesh composed of generalized curved quadrilateral patches—can be used as input to the MOM-SIE method to compute the scattering matrices and polarimetric radar observables on a "drop-by-drop" basis. This will be attempted in the future, and the computations will be compared against those using the "bulk" assumption method and against polarimetric radar measurements. Since we will be computing drop-by-drop scattering matrices to arrive to the radar measurable set using the 2DVD data over a larger time interval involving thousands of different drops, this kind of time averaging (or integration) should yield radar parameters that simulate actual radar observations. In fact, it has been previously demonstrated that drop-by-drop scattering calculations using 2DVD data are indeed feasible and in better agreement with polarimetric radar data relative to using bulk assumptions [*Thurai et al.*, 2009].

6. Conclusions

Drop shapes and oscillation modes have been investigated using 2-D video disdrometer measurements in natural rain at several locations. In the vast majority of the cases, the most probable shapes conform to those

arising from the axisymmetric (2,0) mode. However, there have been a few exceptions, and one example has been illustrated here. The analyses of data from two collocated 2DVD instruments and the C-band polarimetric radar, for the event on 25 December 2009, which had a highly organized line convection embedded within a larger rain system, have shown that mixed-mode oscillations could be inferred within the line, which in turn have been attributed to sustained drop collisions. Inferences have been made from the 2DVD camera data, which showed a substantial fraction of drops undergoing asymmetric mode oscillations (i.e., their images did not possess a rotational axis of symmetry), while the radar data showed much higher than expected differential attenuation within the line.

A number of recent wind tunnel experiments of drop collisions (tiny drops with ~3 mm drops) have shown that the (2,2) and (2,1) mode drop oscillations (of the larger drop) greatly enhance in amplitude immediately upon collision and that these modes can last for up to at least 0.3 s before reverting to its usual (2,0) mode as the dominant mode. If collisions occur typically at a rate of 0.2 s^{-1} (as has been shown in the past), then it is conceivable that collisions can sustain drop oscillations for a significant fraction of such drops.

For oscillating raindrops with asymmetric shapes, scattering calculations using an advanced numerical electromagnetic technique have been performed. The technique implements a method of moments solution to the surface integral equations and enables accurate and efficient scattering matrix calculations of asymmetric hydrometers of electrically large sizes. It has been shown that the scattering matrix and differential reflectivity of drops are dependent on the particular oscillation modes and different time instants within the oscillation cycle. The results have also demonstrated the advantages of the higher-order MOM-SIE method over the DDA method and the T-matrix method in oscillating raindrop analysis.

The MOM-SIE method can be used for computations of polarimetric radar variables using 2DVD-reconstructed 3-D shapes as input to drop-by-drop scattering matrix simulations, thereby enabling more accurate rainfall retrievals and DSDs. Such calculations also enable the spread in cross-polarization discrimination versus CPA to be quantified more accurately for simulated earth-space links operating at microwave and millimeter wave frequencies.

Acknowledgments

This work at Colorado State University was supported by the National Science Foundation under grants AGS-0924622 and AGS-1344862. The authors acknowledge the collaboration with the University of Alabama, Huntsville, and thank the previous and current ARMOR principal investigators, W.A. Petersen and L. Carey, respectively, for supplying the ARMOR data and P. Gatlin for the assistance with the 2DVD maintenance and regular calibrations. The authors also wish to thank M. Szarkall and colleagues at Johannes Gutenberg University of Mainz, Germany, for conducting the wind tunnel experiments reported in this paper and G.-J. Huang of Colorado State University for performing the T-matrix method simulations.

References

Allnutt, J. E. (1989), *Satellite-to-Ground Radiowave Propagation*, Peter Peregrinus Ltd., on behalf of the Inst. of Elect. Eng. (IEE), London, U. K. ISBN: 0863411576.

Amaya-Byrne C. (1995), Depolarisation due to troposphere and its impact on satellite-to-earth communications, PhD thesis, Univ. Catholique de Louvain-la-Neuve, Belgium.

Aresu, A., E. Damosso, A. Martellucci, L. Ordano, and A. Paraboni (1994), Depolarisation of electromagnetic waves due to rain and ice: Theory and experimental results, *Alta Frequenza*, *6*, 70–75.

Beard, K. V. (1984), Oscillation modes for predicting raindrop axis and back scatter ratios, *Radio Sci.*, *19*, 67−74, doi:10.1029/RS019i001p00067.

Beard, K. V., and C. Chuang (1987), A new model for the equilibrium shape of raindrops, *J. Atmos. Sci.*, *44*, 1509–1524.

Beard, K. V., and R. J. Kubesh (1991), Laboratory measurements of small raindrop distortion. Part 2: Oscillation frequencies and modes, *J. Atmos. Sci.*, *48*, 2245−2264.

Beard, K. V., V. N. Bringi, and M. Thurai (2010), A new understanding of raindrop shape, *Atmos. Res.*, *97*, 396−415.

Bringi, V. N., and V. Chandrasekar (2001), *Polarimetric Doppler Weather Radar: Principles and Applications*, 636 pp., Cambridge Univ. Press, Cambridge, U. K.

Brussaard, G. (1976), A meteorological model for rain-induced cross polarization, *IEEE Trans. Antenn. Propag. AP-24*, 5–11.

Chobanyan, E., N. J. Sekeljic, A. B. Manic, M. M. Ilic, and B. M. Notaros (2013a), Atmospheric particle scattering computation using higher order MoM-SIE method, in *Proceedings of the 2013 IEEE Antennas Propag. Soc. Int. Symp.*, Orlando, Fla.

Chobanyan, E., M. M. Ilić, and B. M. Notaroš (2013b), Double-higher-order large-domain volume/surface integral equation method for analysis of composite wire-plate-dielectric antennas and scatterers, *IEEE Trans. Antenn. Propag.*, *61*, 6051−6063.

COST Action 255 (2002), Final Report, *Radiowave Propagation Modelling for New Satellite Communication Services at Ku-band and Above, Part 2 on 'Fixed Propagation Modelling'*, ESA publications Division.

Crowe, C. C., C. J. Schultz, M. R. Kumjian, L. D. Carey, and W. A. Petersen (2012), Use of dual-polarization signatures in diagnosing tornadic potential, *Electron. J. Oper. Meteorol.*, *13*(5), 57–78.

Djordjević, M., and B. M. Notaroš (2004), Double higher order method of moments for surface integral equation modeling of metallic and dielectric antennas and scatterers, *IEEE Trans. Antennas Propag.*, *52*, 2118−2129.

Doviak, R. J., and D. S. Zrnić (1993), *Doppler Radar and Weather Observations*, 2nd ed., 562 pp., Academic Press, San Diego, Calif.

Draine, B. T., and P. J. Flatau (1994), Discrete-dipole approximation for scattering calculations, *JOSA A*, *11*, 1491−1499.

Draine, B. T., and P. J. Flatau (2012), DDSCAT 7.2 code. [Available at http://arxiv.org/abs/1202.3424.]

Feng, J. Q., and K. V. Beard (1991), A perturbation model of raindrop oscillation characteristics with aerodynamic effects, *J. Atmos. Sci.*, *48*, 1856−1868.

Foote G. B. (1973), A numerical method for studying liquid drop behavior: Simple oscillation, *J. Comput. Phys.*, *11*, 417−435.

Goddard, J. W. F., S. M. Cherry, and V. N. Bringi (1982), Comparison of dual-polarization radar measurements of rain with ground-based disdrometer measurements, *J. Appl. Meteorol.*, *21*, 252–256.

Gourley, J. J., A. J. Illingworth, and P. Tabary (2009), Absolute calibration of radar reflectivity using redundancy of the polarization observations and implied constraints on drop shapes, *J. Atmos. Oceanic Tech.*, *26*, 689–703.

Jameson, A. R., and S. L. Durden (1996), A possible origin of linear depolarization observed at vertical incidence in rain, *J. Appl. Meteorol.*, *35*, 271–277.
Jameson, A. R., and A. B. Kostinski (1999), Fluctuation properties of precipitation, Part V: Distribution of rain rates—Theory and observations in clustered rain, *J. Atmos. Sci.*, *56*, 3920–3932.
Johnson, D. B., and K. V. Beard (1984), Oscillation energies of colliding raindrops, *J. Atmos. Sci.*, *41*, 1235–1241.
Kubesh, R. J., and K. V. Beard (1993), Laboratory measurements of spontaneous oscillations for moderate-size raindrops, *J. Atmos. Sci.*, *50*, 1089−1098.
Martellucci, A., and A. Paraboni (1998), Test and development of models of atmospheric crosspolar discrimination for satellite communication systems at Ka and V band, in *Proceedings of the First International Workshop on Radiowave Propagation Modelling for SatCom Services at Ku-band and Above*, ESTEC, Noordwijk, Netherlands.
McFarquhar, G. M. (2004), The effect of raindrop clustering on collision-induced break-up of raindrops, *Q. J. R. Meteorol. Soc.*, *130*, 2169–2190.
Mishchenko, M. I., L. D. Travis, and A. A. Lacis (2002), *Scattering, Absorption, and Emission of Light by Small Particles*, Cambridge Univ. Press, Cambridge, U. K.
Notaroš, B. M. (2008), Higher order frequency-domain computational electromagnetics, Invited review paper, Special Issue on Large and Multiscale Computational Electromagnetics, *IEEE Trans. Antennas Propag.*, *56*, 2251−2276.
Oguchi, T. (1983), Electromagnetic wave propagation and scattering in rain and other hydrometeors, *Proc. IEEE*, *71*, 1029–1078.
Okamura, S., and T. Oguchi (2010), Electromagnetic wave propagation in rain and polarization effects, *Proc. Jpn. Acad. Ser. B Phys. Biol. Sci.*, *86*(6), 539–562.
Petersen, W. A., K. R. Knupp, D. J. Cecil, and J. R. Mecikalski (2007), The University of Alabama Huntsville THOR Center instrumentation: Research and operational collaboration, Preprints, paper 5.1. presented at 33rd Conference on Radar Meteorology, Am. Meteorol. Soc., Cairns, Australia. [Available at https://ams.confex.com/ams/33Radar/webprogram/Paper123410.html.]
Pruppacher, H. R. (1988), Auswaschen von atmosphärischen Spurenstoffen durch Wolken und Niederschlag mittels eines vertikalen Windkanals, (Scavenging of trace gases by clouds and precipitation using a vertical wind tunnel.) *Gesellschaft für Strahlen- und Umweltforschung*, BPT-Bericht 9/88, 62 pp.
Ray, P. S. (1972), Broadband complex refractive indices of ice and water, *Appl. Optics*, *11*(8), 1836–1844.
Rogers, R. R. (1989), Raindrop collision rates, *J. Atmos. Sci.*, *46*, 2469–2472.
Schönhuber, M., W. L. Randeu, H. E. Urban, and J. P. V. Poiares Baptista (2000), Field measurements of raindrop orientation angles, in *Proc. AP2000 Millennium Conf. on Antennas and Propagation*, IEE, CD-ROM, Davos, Switzerland.
Schönhuber, M., G. Lammer, and W. L. Randeu (2008), The 2D-video-vistrometer, Chapter 1, in *Precipitation: Advances in Measurement, Estimation and Prediction*, edited by S. Michaelides, Springer, ISBN: 978-3-540-77654-3.
Sekeljic, N. J., A. B. Manic, E. Chobanyan, M. Thurai, V. N. Bringi, and B. M. Notaros (2014), Electromagnetic scattering by oscillating rain drops of asymmetric shapes, paper presented at 2014 IEEE Antennas and Propagation Society International Symposium, IEEE, Memphis, Tenn.
Sheppard, B. E. (1990), The measurement of raindrop size distributions using a small Doppler radar, *J. Atmos. Oceanic Tech.*, *7*, 255–268.
Szakáll, M., K. Diehl, S. K. Mitra, and S. Borrmann (2009), A wind tunnel study on the shape, oscillation, and internal circulation of large raindrops with sizes between 2.5 and 7.5 mm, *J. Atmos. Sci.*, *66*, 755−765.
Szakáll, M., K. Diehl, S. K. Mitra, and S. Borrmann (2010), Shapes and oscillations of falling raindrops—A review, *Atmos. Res.*, *97*, 416−425.
Szakáll, M., S. Kessler, K. Diehla, S. K. Mitra, and S. Borrmann (2014), A wind tunnel study of the effects of collision processes on the shape and oscillation for moderate-size raindrops, *Atmos. Res.*, *142*(1), 67–78, doi:10.1016/j.atmosres.2013.09.005.
Teschl, F., W. L. Randeu, and R. Teschl (2013), Single-scattering of preferentially oriented ice crystals at centimeter and millimeter wavelengths, *Atmos. Res.*, *119*, 112–119, doi:10.1016/j.atmosres.2011.10.004.
Thurai, M., and V. N. Bringi (2005), Drop axis ratios from a 2D video disdrometer, *J. Atmos. Oceanic Tech.*, *22*, 966−978.
Thurai, M., and V. N. Bringi (2013), Recent measurements and inferences of drop shapes in rain from 2D-video disdrometer and polarimetric radar, *Space Comm.*, *22*, 171–178, doi:10.3233/SC-130012.
Thurai, M., G. J. Huang, V. N. Bringi, W. L. Randeu, and M. Schönhuber (2007), Drop shapes, model comparisons, and calculations of polarimetric radar parameters in rain. *J. Atmos. Oceanic Tech.*, *24*, 1019−1032.
Thurai, M., V. N. Bringi, and W. A. Petersen (2009), Rain microstructure retrievals using 2-D video disdrometer and C-band polarimetric radar, *Adv. Geosci.*, *20*, 13−18.
Thurai, M., M. Szakall, V. Bringi, and S. K. Mitra (2013a), Collision-induced drop oscillations from wind-tunnel experiments, Preprints, paper 9B.2. presented at 36th Conference on Radar Meteorology, Am. Meteorol. Soc., Breckenridge, Colo. [Available at https://ams.confex.com/ams/36Radar/webprogram/Paper228158.html.]
Thurai, M., V. N. Bringi, W. A. Petersen, P. N. Gatlin (2013b), Drop shapes and fall speeds in rain: two contrasting examples, *J. Appl. Meteorol. Climatol.*, *52*, 2567−2581.
Thurai, M., V. N. Bringi, A. B. Manić, and B. M. Notaroš (2013c), Ongoing investigations of rain drop shapes and oscillation modes, in *Proc. URSI Commission F Triennial Open Symposium on Radiowave Propagation and Remote Sensing*, Ottawa, Canada.
Thurai, M., P. N. Gatlin, V. N. Bringi, and L. Carey (2014), Very large rain drops from 2D video disdrometers and concomitant polarimetric radar observations, Extended abstract, paper presented at 8th European Conference on Radar in Meteorology and Hydrology, Garmisch-Partenkirchen, Germany, 1–5 Sept.
Van de Kamp, M. M. J. (2004), Separation of simultaneous rain and ice depolarization, *IEEE Trans. Antennas Propag.*, *52*(2), 513–523.